Design Concept and Preliminary Experimental Demonstration of MEMS Gyroscopes with 4-DOF "Master-Slave" Architecture

Cenk Acar and Andrei M. Shkel

Microsystems Laboratory, Department of Mechanical and Aerospace Engineering
University of California at Irvine, CA, USA

ABSTRACT

This paper reports a design concept for MEMS gyroscopes that shifts the complexity of the design from control architecture to system dynamics, utilizing the passive disturbance rejection capability of the 4-DOF dynamical system. Specifically, a novel wide-bandwidth micromachined gyroscope design approach based on increasing the degrees-of-freedom of the oscillatory system by the use of two independently oscillating interconnected proof masses is presented along with preliminary experimental demonstration of implementation feasibility. With the concept of using a 4-DOF system, inherent disturbance rejection is achieved due to the wide operation frequency range of the dynamic system, providing reduced sensitivity to structural and thermal parameter fluctuations. Thus, less demanding active control strategies are required for operation under presence of perturbations. The fabricated prototype dual-mass gyroscopes successfully demonstrated a dramatically wide driving frequency range within where the drive direction oscillation amplitude varies insignificantly without any active control, in contrast to the conventional gyroscopes where the mass has to be sustained in constant amplitude oscillation in a very narrow frequency band. Mechanical amplification of driven mass oscillation by the sensing element was also experimentally demonstrated, providing large oscillation amplitudes, which is crucial for sensor performance.

Keywords: MEMS, inertial sensors, micromachined gyroscopes

1. INTRODUCTION

The conventional micromachined rate gyroscopes operate on the vibratory principle of a 2 degrees-of-freedom (DOF) system with a single proof mass suspended by flexures anchored to the substrate, which make the mass free to oscillate in two orthogonal directions, namely the drive and the sense directions. The proof mass is

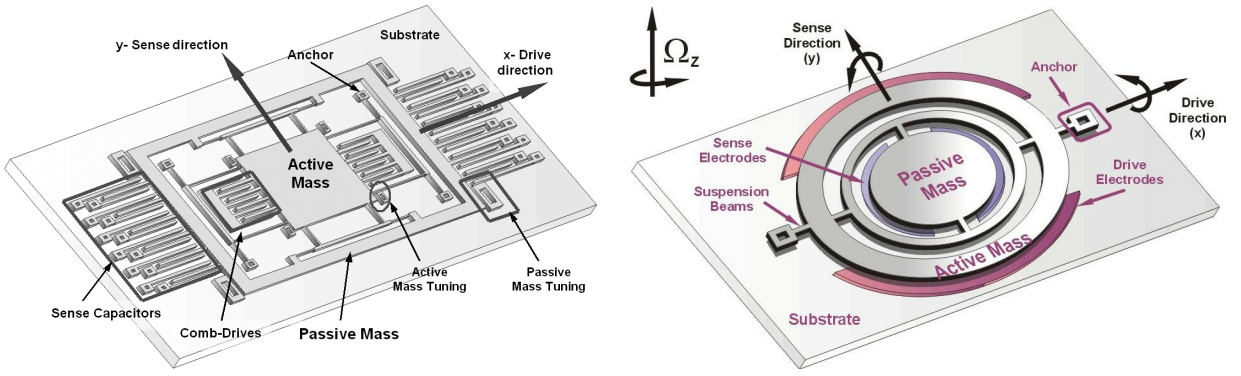

Figure 1. (a) Linear, and (b) Torsional implementation of the 4-DOF "Master-Slave" design concept. The master mass is electrostatically driven to achieve mechanical amplification by the slave mass, and the Coriolis response of the slave mass in the sense direction is detected.

Further author information: (Send correspondence to C.A.)
C.A.: E-mail: cacar@uci.edu
A.S.: E-mail: ashkel@uci.edu
Web: http://mems.eng.uci.edu

sustained in resonance in drive direction, and in the presence of an angular rotation, the Coriolis force proportional to the input angular rate is induced, exciting the proof mass in the sense direction. To achieve high gain, the drive and the sense resonant frequencies are typically designed to match, and the device is controlled to operate at the peak of their response curve. However, this resonance dependent approach results in high sensitivity to variations in system parameters. Only 1% shift in resonance frequency might produce over 20% error in the output signal gain, while major dynamical system parameters were observed to be likely to deviate by up to 15% from theoretical and numerical models in basic experiments conducted on various fabricated gyroscopes. In addition, the 2-DOF system gain is affected significantly by fluctuations in damping. Thus, sophisticated control electronics is required for constant amplitude operation in the region of the resonance peak (Fig. 3).[5]

In order to overcome the drawbacks of the conventional micromachined gyroscope approach, we propose a design concept incorporating a vibratory system with increased degrees-of-freedom, providing a more favorable frequency response. In contrast to the conventional micromachined gyroscopes, the proposed design approach utilizes a "master" and a "slave" proof mass, which are free to oscillate both in the drive and sense directions (Fig. 1), forming a 4-DOF dynamic system (Fig. 2a). The master mass, also called the active mass, is forced to oscillate in the drive direction, and this forced oscillation is amplified by the slave mass, which is thus called the passive mass. The response of the passive mass to the Coriolis force in the orthogonal direction is sensed. Due to the increased dimensionality of the dynamic system, a Coriolis response with two resonant peaks, and a flat region between peaks can be obtained (Fig. 2b). Nominal operation of the device is in the flat region of the response, where the gain is relatively insensitive to parameter fluctuations. Thus, the device can be operated in a much wider frequency band with insignificant change in the gain, providing an inherent robustness against perturbations in dynamical system parameters.[7]

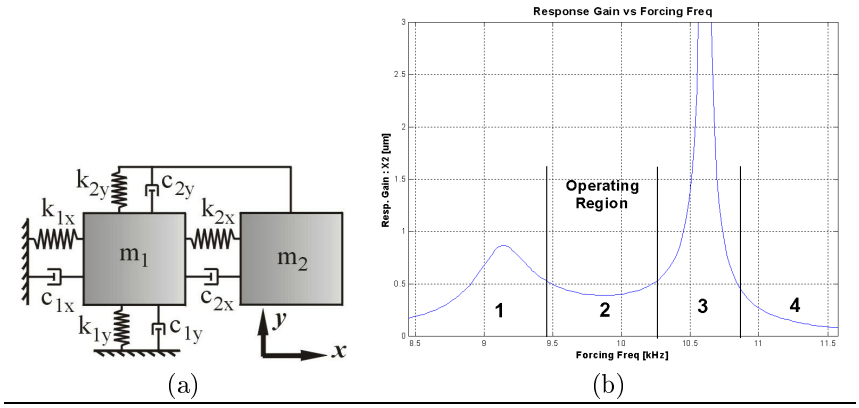

Figure 2. (a) Lumped parameter model of the 4-DOF gyroscope. The "slave mass" is coupled to the "master mass" in both the drive and the sense directions. (b) Response of the dual-mass system with the flat operating region.

In this paper, in order to form a basis of comparison between the conventional and 4-DOF gyroscopes, we first present a detailed analysis of the conventional gyroscope dynamics together with investigation of oscillation pattern issues affected by phase relations and anisoelasticity in the suspension structure. Then, the 4-DOF gyroscope design concept is presented along with system dynamics and an approach for determining optimal system parameters to maximize sensor performance. The phase relations in the ideal and non-ideal 4-DOF system is also analyzed to obtain mass trajectories in oder to compare with the conventional systems from the Quadrature control point of view. Finally, preliminary experimental results verifying the major operational principles of the 4-DOF gyroscope are presented.

2. CONVENTIONAL GYROSCOPE APPROACH

Almost all reported micromachined rate gyroscopes operate on the vibratory principle of a single proof mass suspended above the substrate. The proof mass is supported by anchored flexures, which serve as the flexible suspension between the proof mass and the substrate, making the mass free to oscillate in two orthogonal directions (Fig. 3): the drive direction, x-Axis, and the sense direction, y-Axis.[2] The overall dynamical system is simply a 2-DOF mass-spring-damper system, where the drive direction is excited by the electrostatic drive forces, and the sense direction is excited by the rotation-induced Coriolis force. The equations of motion along the two principle oscillation axes, the drive direction x and the sense direction y, can be expressed as:

$$m\ddot{x} + c_x\dot{x} + (k_x - m({\Omega_y}^2 + {\Omega_z}^2))x + m(\Omega_x\Omega_y - \dot{\Omega_z})y = F_d + 2m\Omega_z\dot{y}$$
$$m\ddot{y} + c_y\dot{y} + (k_y - m({\Omega_x}^2 + {\Omega_z}^2))y + m(\Omega_x\Omega_y + \dot{\Omega_z})x = -2m\Omega_z\dot{x}. \quad (1)$$

The two final terms $2m\Omega_z\dot{y}$ and $2m\Omega_z\dot{x}$ in the equation are the rotation-induced Coriolis forces, which cause dynamic coupling between the oscillation axes, and which are used for angular rate measurement. In most of the reported micromachined vibratory rate gyroscopes, the proof mass is driven into resonance in the drive direction by an external sinusoidal force. When the gyroscope is subjected to an angular rotation, the Coriolis force is induced in the y-direction. If the drive and sense resonant frequencies are matched, the Coriolis force excites the system into resonance in the sense direction, as well. The resulting oscillation amplitude in the sense direction is proportional to the Coriolis force and, thus, to the angular velocity to be measured.[2]

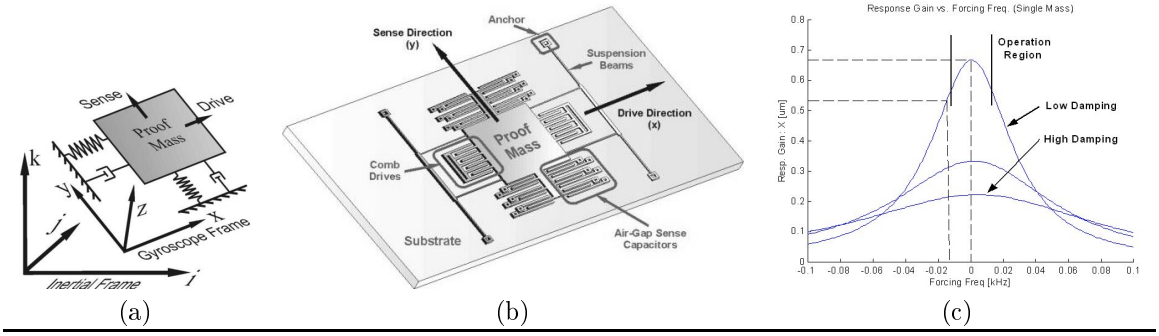

(a) (b) (c)

Figure 3. (a) Schematic of the conventional 2-DOF gyroscope dynamical model. (b) A conceptual MEMS implementation of a conventional rate gyroscope. (c) The device detects the response in the sense direction excited by the Coriolis force.

A better insight to the dynamics of the single-mass 2-DOF gyroscope can be acquired by starting with the assumption that the system is driven without feedback control in drive direction x with a constant amplitude drive force F_d at the drive frequency ω_d, namely $F_d = F_o sin\omega_d t$. For a constant angular rate input, i.e. $\dot{\Omega}_z = 0$, and for angular rates much lower than the driving frequency of the gyroscope, the equations of motion reduce to:

$$m\ddot{x} + c_x\dot{x} + k_x x = F_o sin\omega_d t + 2m\Omega_z\dot{y}$$
$$m\ddot{y} + c_y\dot{y} + k_y y = -2m\Omega_z\dot{x}. \quad (2)$$

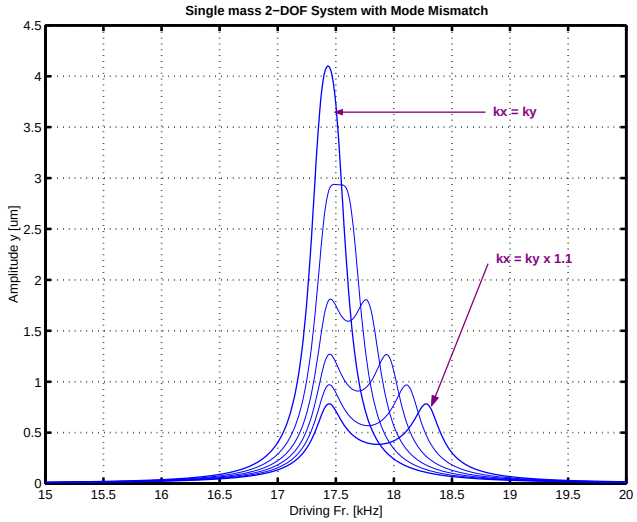

Figure 4. The response of the overall 2-DOF system with varying drive and sense stiffness mismatch. The highest response corresponds to the case where the drive and sense modes are matched, and the response amplitude diminishes as the mismatch increases.

The 2-DOF dynamical system will have two independent resonant frequencies: drive direction resonant frequency ω_x, and sense direction resonant frequency ω_y. When the stiffness values in the drive and sense directions are the same, i.e. $k_x = k_y$ then the two resonance modes will be matched, i.e. $\omega_x = \omega_y$. However, fabrication imperfections are inevitable, and both the geometry and the material properties of MEMS devices are affected by etching processes, deposition conditions, and residual stresses, drastically affecting the suspension stiffness. Generally, sophisticated control electronics is used to tune the resonance frequencies for mode-matching.

The rotation-induced Coriolis force $F_c = 2m\Omega_z\dot{x}$, which is proportional to the drive direction oscillation amplitude is the only driving force in the sense direction. Denoting x_o and y_o as the drive and sense direction oscillation amplitudes respectively, it can be observed that the sense direction amplitude is proportional to the Coriolis force F_c, and thus to the drive direction oscillation amplitude. If $\omega_d = \omega_y$, then system is in resonance in the sense direction, and a high sense direction amplitude is expected due to sense direction resonance. If $\omega_d = \omega_x$, then system is in resonance in the drive direction, and a high sense direction amplitude is expected due to the increased Coriolis force F_c in the drive direction resonance. Thus, when $\omega_x \neq \omega_y$, the frequency response of the 2-DOF system has two resonant peaks, one at ω_x, and one at ω_y. When $\omega_x = \omega_y$, the frequency response of the 2-DOF system has one combined resonant peak, which will provide a much larger response amplitude due to coinciding drive and sense resonance peaks (Fig. 4).

2.1. Phase Relations and Proof-Mass Trajectory

In an ideal single-mass MEMS gyroscope, the oscillation pattern of the mass in the plane of the substrate depends on the phase difference between its drive and sense direction responses. The steady state response of the simplified 2-DOF system (2) will be a coupled harmonic oscillator of the form:

$$\begin{aligned} x(t) &= x_o sin\omega_d t + \phi_x \\ y(t) &= y_o sin\omega_d t + \phi_y \end{aligned} \tag{3}$$

where x_o and y_o are the drive and sense direction amplitudes respectively, and ϕ_x and ϕ_y are the drive and sense response phases. If the phase difference $\phi_y - \phi_x = 180^o$, then the steady-state trajectory is a straight line (Fig. 5a), which is the expected response of an ideal gyroscope. The slope of the straight line depends solely on the Coriolis force, thus the input rotation. Since y_o is also proportional to x_o ($y_o \propto F_c \propto x_o$), the slope of the straight line of oscillation does not depend on drive direction oscillation amplitude. If the phase difference $\phi_y - \phi_x \neq 180^o$, then the trajectory turns into an ellipse, which means y does not have its maximum where x is in its extreme points (Fig. 5b). Thus the oscillation pattern deviates from a straight line. The sense direction amplitude of the resulting elliptic oscillation is proportional to the Coriolis force, thus to the input rotation. However, the elliptic oscillation pattern will interfere with phase-dependent detection or control techniques.

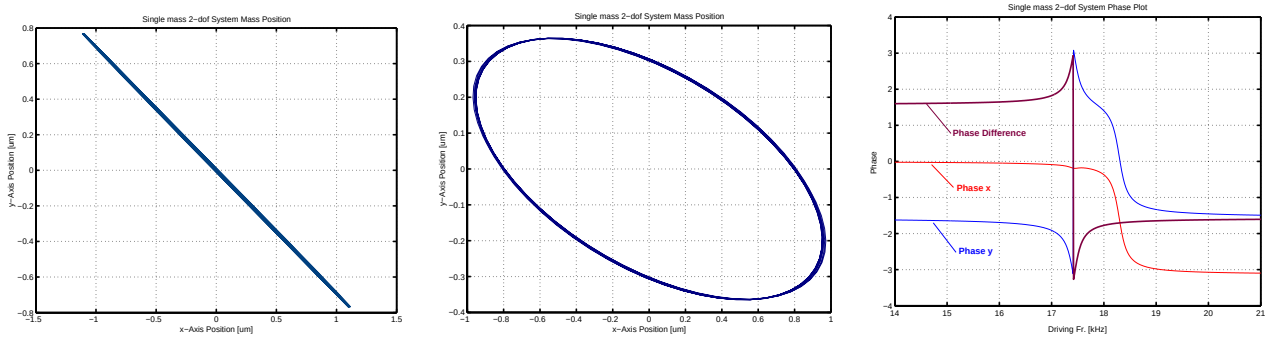

(a) (b) (c)

Figure 5. (a) The oscillation pattern when $\omega_d = \omega_y$. (b) The oscillation pattern when $\omega_d \neq \omega_y$. (c) Phase relations in x and y directions. The phase difference $\phi_y - \phi_x$ does not depend on the the drive direction resonant frequency ω_x. The phase difference is determined solely by $\omega_d - \omega_y$.

When the system is driven along x-axis with a constant amplitude drive force at the drive frequency ω_d, there will be a phase difference ϕ_x between the deflection and the force. The phase depends on the location of the driving frequency relative to the resonance peak, namely the quantity $\omega_d - \omega_x$. If $\omega_d = \omega_x$, then the system is in resonance in drive direction, and the phase difference ϕ_x between the deflection and the force is 90^o (Fig. 5c).

Similarly, since Coriolis force F_c is the driving force in the sense direction, the sense direction deflection phase depends on the location of the driving frequency relative to the sense direction resonance peak, namely the quantity $\omega_d - \omega_y$. If $\omega_d = \omega_y$, then the system is in resonance in the sense direction, and the phase difference ϕ_y between the sense direction deflection and the Coriolis force is 90^o. However, it should be noticed that the Coriolis force F_c is proportional to the drive direction velocity $\dot{x}$, and it is always in phase with $\dot{x}$. Thus, F_c is always 90^o phase shifted from drive direction displacement x, regardless of the driving frequency.

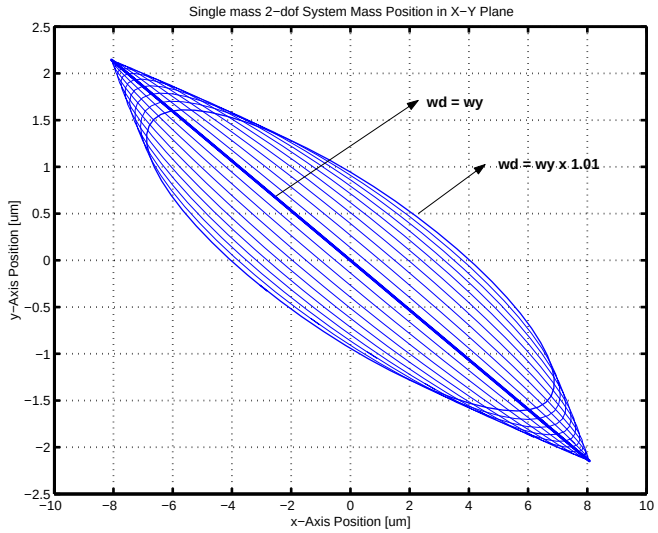

Figure 6. Transformation of the straight line of oscillation into an ellipse as the driving frequency ω_d deviates from the sense direction resonant frequency ω_y.

Consequently, phase difference between the drive and sense direction responses $(\phi_y - \phi_x)$ does not depend on the location of the driving frequency with respect to ω_x. In other words, the mass trajectory is independent of $\omega_d - \omega_x$. The only frequency relation determining the trajectory is $\omega_d - \omega_y$. If $\omega_d = \omega_y$, then the drive and sense phase difference $(\phi_y - \phi_x)$ is 180^o because of 90^o phase shift between F_c and $x(t)$, and 90^o phase shift due to resonance between sense deflection $y(t)$ and the sense direction driving force F_c. Thus, when the system is driven at the sense direction resonant frequency, and the trajectory is a straight line. When the driving frequency ω_d deviates from ω_y, the trajectory turns into an ellipse (Fig. 6).

2.2. Anisoelasticity and Quadrature Error Issues

Fabrication imperfections and residual stresses in MEMS gyroscopes cause drive and sense direction stiffness mismatches, which result in minimum and maximum-stiffness axes in the plane of oscillation. Furthermore, the minimum and maximum-stiffness axes are likely to deviate from the drive and sense oscillation directions because of slight asymmetries in structure due to random scatter of imperfections. Due to lack of perfect alignment of the intended and the actual principle axes of oscillation, anisoelasticity in the gyroscope structure occurs, causing dynamic cross-coupling between the drive and sense directions. The resulting dynamic cross-coupling stiffness and damping terms are the major factors that limit the performance of the gyroscope.[9]

Deviation of the main axes of elasticity introduces position-dependent coupling forces between the drive and sense direction transforming the straight line of oscillation to an ellipse (Fig. 7a). Since the coupling anisoelastic forces are in phase with the position, the resulting ellipse trajectory has a different profile than effect of x-y oscillation phase difference. It can also be observed that an angle of anisoelasticity results in the same elliptic deviation regardless of the spring constant mismatch (Fig. 8a), even though stiffness mismatch is the main reason of quadrature error together with anisoelasticity. In the absence of an input angular velocity, the position-dependent anisoelastic forces cause an elliptic oscillation pattern with a response proportional to angle of anisoelasticity (Fig. 7b, c).

When the driving frequency is deviated from the resonant frequency of the sense direction, the mass trajectory is already an ellipse without any anisoelasticity. Furthermore, as the drive and sense phase difference $(\phi_y - \phi_x)$ deviates from 180^o to 90^o, the Coriolis response has the same phase as the Quadrature error, and the Coriolis signal becomes indistinguishable from the Quadrature signal using phase-related filtering techniques.

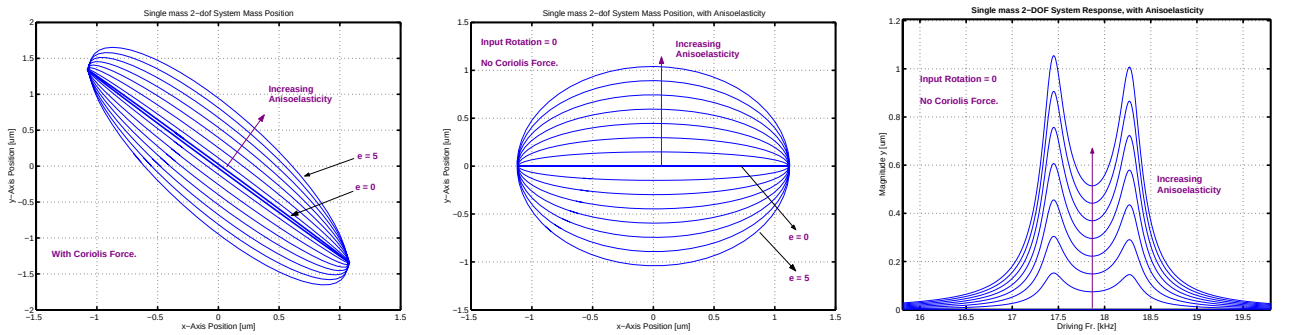

Figure 7. (a) Deviation of the elliptic oscillation pattern due to increasing anisoelasticity. (b) Effect of anisoelasticity on the straight line of oscillation along x-axis with zero input rotation rate. (c) In the absence of input rate, anisoelasticity induces a sense direction response similar to the Coriolis response.

At high quality factors, this is likely to occur with very small frequency mismatches due to the very abrupt change in phase. If anisoelasticity is introduced to the case where the oscillation is already an ellipse, the slope of the ellipse axes changes, while the drive and sense direction oscillation amplitudes vary insignificantly (Fig. 8b).

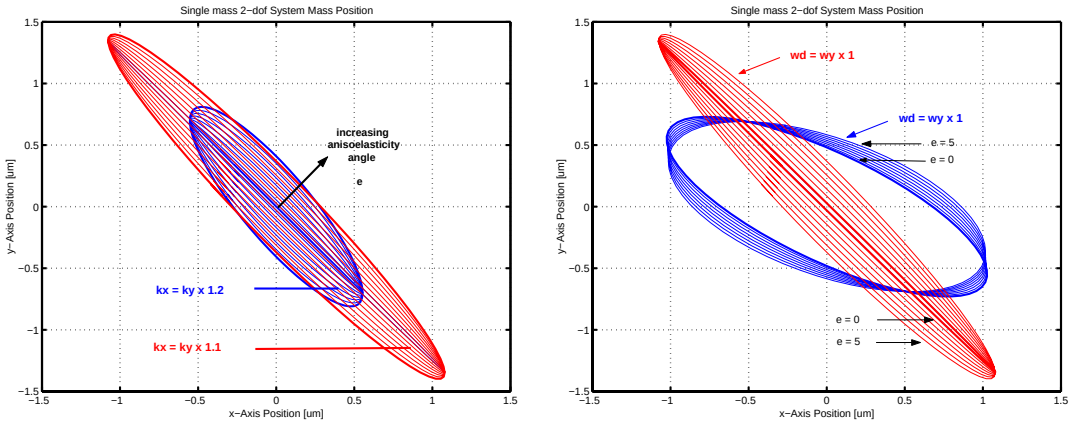

Figure 8: Effect of anisoelasticity on (a) stiffness mismatched systems, and (b) systems with ω_d deviated from ω_y.

Consequently, all the explained factors limit the performance of the conventional gyroscopes since the system is very sensitive to variations in system parameters that shift the drive or sense resonant frequencies. Under high quality factor conditions the gain is high, however, the bandwidth is extremely narrow, which also results in abrupt phase changes. In addition, the gain and the phases are affected significantly by fluctuations in damping conditions. Compensation for these effects require a very complicated control architecture.

3. THE 4-DOF SYSTEM APPROACH

To eliminate the limitations of the conventional micromachined gyroscopes, we propose a design concept that suggests the use of an oscillatory system with increased parametric space, providing a more favorable frequency response. The proposed design concept is based on increasing the degrees-of-freedom of the oscillatory system by the use of two independently oscillating interconnected proof masses. With the 4-DOF system, inherent disturbance rejection is achieved due to the wide operation frequency range of the dynamic system, providing reduced sensitivity to structural and thermal parameter fluctuations. With the new design concept that requires less demanding active control strategies for operation under presence of perturbations, complexity of the control electronics can be shifted to dynamical system complexity. Thus, the approach is expected to provide low-cost solutions to applications with high operation condition fluctuations, where self-calibration is crucial.

In contrast to the conventional micromachined gyroscopes, the proposed design approach utilizes two vibrating proof masses suspended above the substrate, which form a 4 degrees-of-freedom (DOF) dynamic system

(Fig. 2a). The suspension system renders both of the proof masses free to oscillate in the drive and sense directions. The first mass is forced to oscillate in the drive direction, and this forced oscillation is amplified by the second mass. The response of the second mass to the Coriolis force in the orthogonal direction is sensed. With appropriate selection of dynamical system parameters, a Coriolis response with two resonant peaks, and a flat region between peaks can be obtained. Nominal operation of the device is in the flat region of the response, where the gain is relatively insensitive to parameter fluctuations (Fig. 2b). In this flat region, a 1% variation in natural frequencies of the system results in only 0.8% error in the output signal, which is less than 4% of the error experienced with a conventional design under similar operating conditions. Thus, the device can be operated in a much wider frequency band with insignificant change in the gain. Moreover, since the proposed device utilizes dynamic amplification of mechanical motion instead of in-resonance operation, the response is insensitive to damping changes in the operation region.[7]

3.1. 4-DOF System Dynamics

When the active and passive masses are observed in the non-inertial rotating gyroscope frame, additional inertial forces appear acting on both masses. Since both masses are subject to an angular rate of Ω_z about the axis normal to the plane of operation (z-axis), the equations of motion for the two-mass system along the x-axis and y-axis become[7]:

$$\begin{aligned}
m_1\ddot{x_1} + c_{1x}\dot{x_1} + k_{1x}x_1 &= k_{2x}(x_2 - x_1) + c_{2x}(\dot{x_2} - \dot{x_1}) + m_1\Omega_z^2 x_1 - 2m_1\Omega_z\dot{y_1} - m_1\dot{\Omega}_z y_1 + F_d(t) \\
m_2\ddot{x_2} + c_{2x}(\dot{x_2} - \dot{x_1}) + k_{2x}(x_2 - x_1) &= m_2\Omega_z^2 x_2 - 2m_2\Omega_z\dot{y_2} - m_2\dot{\Omega}_z y_2 \\
m_1\ddot{y_1} + c_{1y}\dot{y_1} + k_{1y}y_1 &= k_{2y}(y_2 - y_1) + c_{2y}(\dot{y_2} - \dot{y_1}) + m_1\Omega_z^2 y_1 + 2m_1\Omega_z\dot{x_1} + m_1\dot{\Omega}_z x_1 \\
m_2\ddot{y_2} + c_{2y}(\dot{y_2} - \dot{y_1}) + k_{2y}(y_2 - y_1) &= m_2\Omega_z^2 y_2 + 2m_2\Omega_z\dot{x_2} + m_2\dot{\Omega}_z x_2. \qquad (4)
\end{aligned}$$

where $F_d(t)$ is the driving electrostatic force applied to the active mass at the driving frequency ω_d, and Ω_z is the angular velocity applied to the gyroscope about the z-axis.

3.2. Design Implementations

Depending on the parameters of the fabrication process, the 4-DOF design concept can be implemented in various geometries. When a fabrication technology with a high structural polysilicon thickness is used, a linear design is preferred (Fig. 1a), since large actuation forces and large sense capacitances can be achieved with the increased thickness in the comb-drives and the air-gap capacitors.

When a surface micromachining technology with a small structural layer thickness is used, a torsional design (Fig. 1b) will be more advantageous. The active mass, which is the outermost ring, will be torsionally driven about the x-axis, and its motion will be amplified by the passive mass to obtain large torsional oscillations about the x-axis. When the device is subject to an angular rate about the axis normal to the substrate, Coriolis torques will be induced on the passive mass, driving the gimbal system into torsional oscillations about the y-axis, which will be detected by the large differential parallel-plate electrodes underneath the passive mass.

3.3. Parameter Optimization in the Drive Mode

The gyroscope is simply a 2-DOF system in the drive mode. The drive force is applied to the first mass by the comb drive structures. Approximating the gyroscope by a lumped mass-spring-damper model (Figure 9), the equations of motion in the drive direction can be expressed as:

$$\begin{aligned}
m_1\ddot{x_1} + c_{1x}\dot{x_1} + k_{1x}x_1 &= k_{2x}(x_2 - x_1) + F_{drive} \\
m_2\ddot{x_2} + c_{2x}\dot{x_2} + k_{2x}x_2 &= k_{2x}x_1. \qquad (5)
\end{aligned}$$

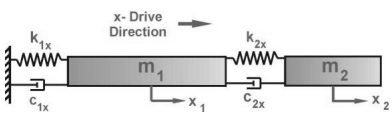

Figure 9: Drive mode lumped mass-spring-damper model of a dual-mass gyroscope.

Since the foremost mechanical factor determining the performance of the gyroscope is the sense direction deflection of the passive mass due to the input rotation, the parameters of the dynamical system should be optimized to maximize the oscillation amplitude of the passive mass in the sense direction. Due to mechanical amplification in the drive mode, oscillation amplitudes of the active mass is much smaller compared to the passive mass, which generates a much smaller Coriolis Force on the active mass. Thus, the dominant force that drives the system in sense direction is the Coriolis force induced on the passive mass. This requires determining an optimal m_2 according to Coriolis Force requirement as the first step.

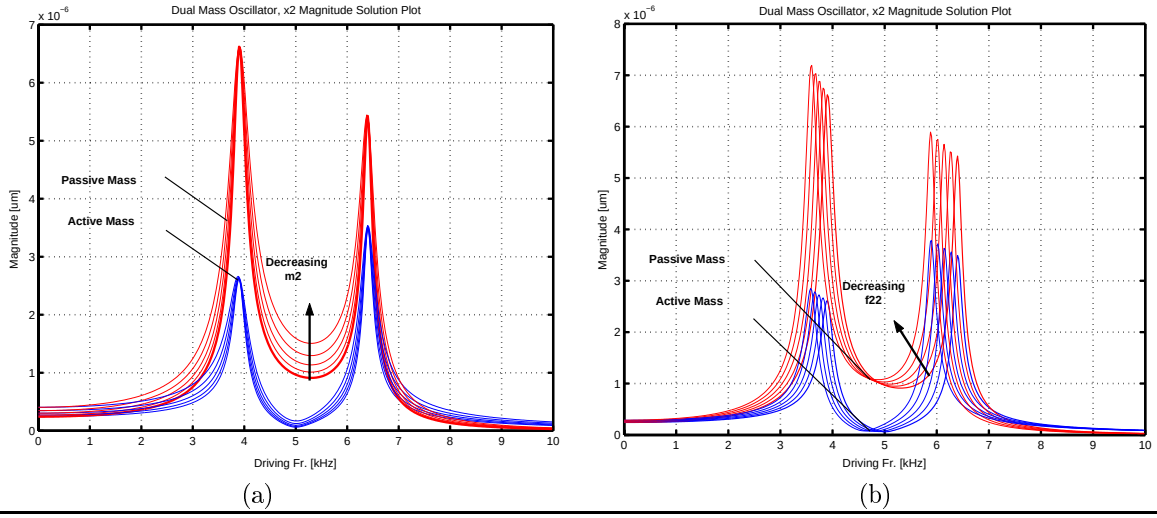

(a) (b)

Figure 10. Effect of (a) passive mass m_2 variation, and (b) antiresonant frequency ω_{22} variation on drive direction response.

For a high enough Coriolis Force $2m_2\Omega_z\dot{x}_2$ acting on the passive mass, which will drive the system in sense direction, m_2 has to be large. However, if the response of the passive mass in the drive direction is observed for varying m_2 values, it is seen that for high oscillation amplitudes of passive mass, m_2 has to be as small as possible (Fig. 10a). Thus, an optimal passive mass is selected based on these criteria.

As the second step, the resonant frequency ω_{22} of the isolated passive mass-spring system is determined according to gyroscope operating frequency specifications. It should be noticed that larger Coriolis forces are induced at higher frequencies, but the oscillation amplitudes become larger at lower frequencies (Fig. 10b). Once ω_{22} is fixed, the drive direction spring constant k_{2x} of the passive mass is obtained from ω_{22} and m_2.

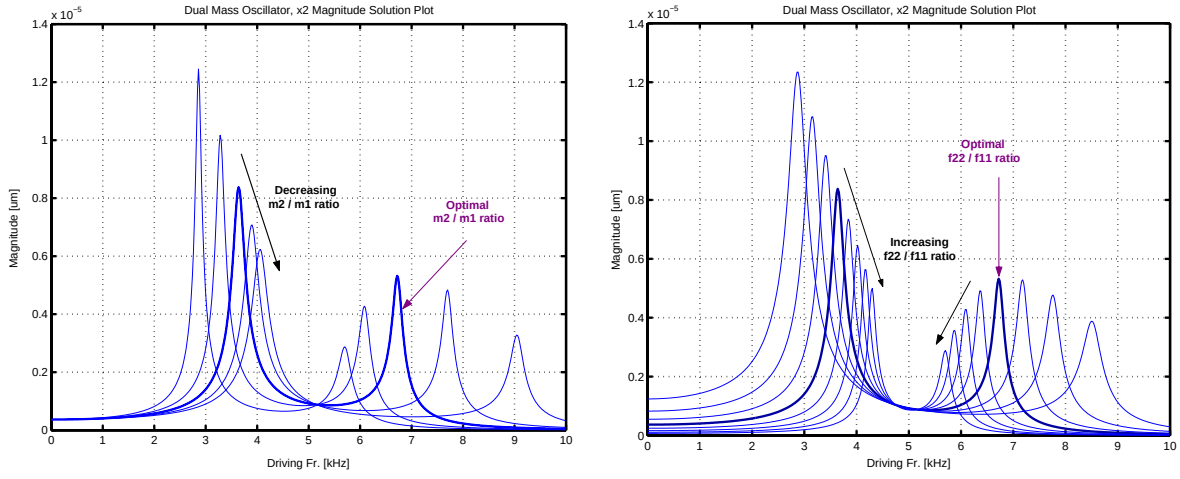

(a) (b)

Figure 11. Effect of (a) mass ratio $\mu = m_2/m_1$ variation, and (b) frequency ratio $\gamma = \omega_{22}/\omega_{11}$ variation on drive direction response.

To determine the mass of the active mass, an optimal mass ratio $\mu = m_2/m_1$ has to be found. In order to achieve insensitivity to damping, the resonance peaks of the 2-DOF system response have to be separated enough, which imposes a minimum value for μ. For a wide bandwidth, again a large μ is required for enough separation of the peaks; however, to prevent gain drop, the peak separation should be narrow enough (Fig. 11a).

The degree of mechanical amplification depends on the ratio of the isolated active and passive mass-spring systems, namely $\omega_{11} = \sqrt{k_{1x}/m_1}$ and $\omega_{22} = \sqrt{k_{2x}/m_2}$. The optimal frequency ratio $\gamma = \omega_{22}/\omega_{11}$ has to be determined such that γ is high enough for high mechanical amplification, and high oscillation amplitudes of passive mass (Fig. 11b). From the optimal values of ω_{11} and μ the drive direction spring constant k_{1x} of the active mass is obtained. Finally, the damping conditions of the overall device have to be checked to verify that damping values are in the region where the response gain in the antiresonance region is insensitive to damping variations (Fig. 12).

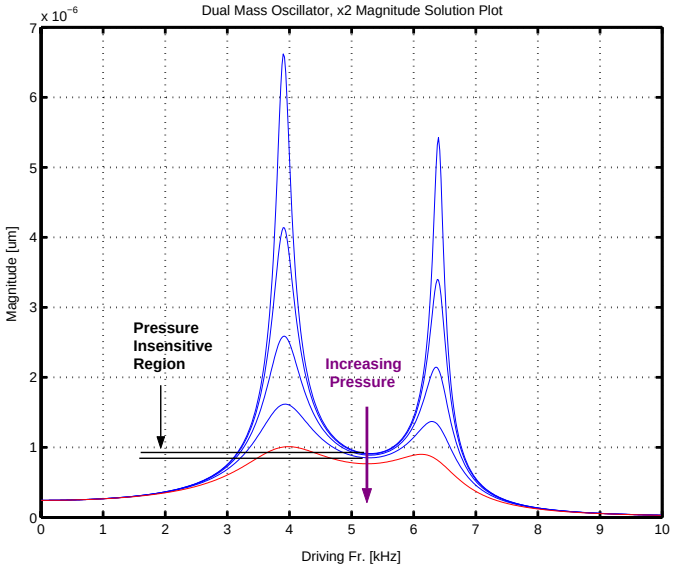

Figure 12. Effect of damping on drive direction response. When the damping is under a critical value, the response in the flat region is insensitive to pressure changes.

3.4. Phase Relations and Effects of Anisoelasticity

When the system is driven in the flat operating region near the drive direction antiresonant frequency, drive direction position of the active mass x_1 is 90^o in phase with the electrostatic drive force F_d. With mechanical amplification, drive direction position of the passive mass x_2 is greater than x_1, and is 90^o in phase with x_1. The Coriolis forces F_{c1} and F_{c2} acting on the active mass and the passive mass respectively are again proportional to the linear velocities of the masses, and thus they are 90^o in phase with the related positions x_1 and x_2, respectively. Since the amplitude of the passive mass is much greater than the active mass, the dominant force that drives the system in sense direction is F_{c2}, which is 90^o in phase with x_2. Thus, the force-position phase relation in sense direction determines the profile of the mass trajectories.

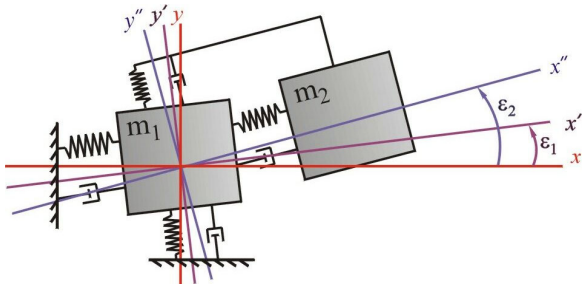

Figure 13. Modeling of asymmetric imperfections in the 4-DOF gyroscope. The asymmetric imperfections can be modeled as an angle of elasticity ε_1 for substrate-active mass suspension, and ε_2 for active mass-passive mass suspension.

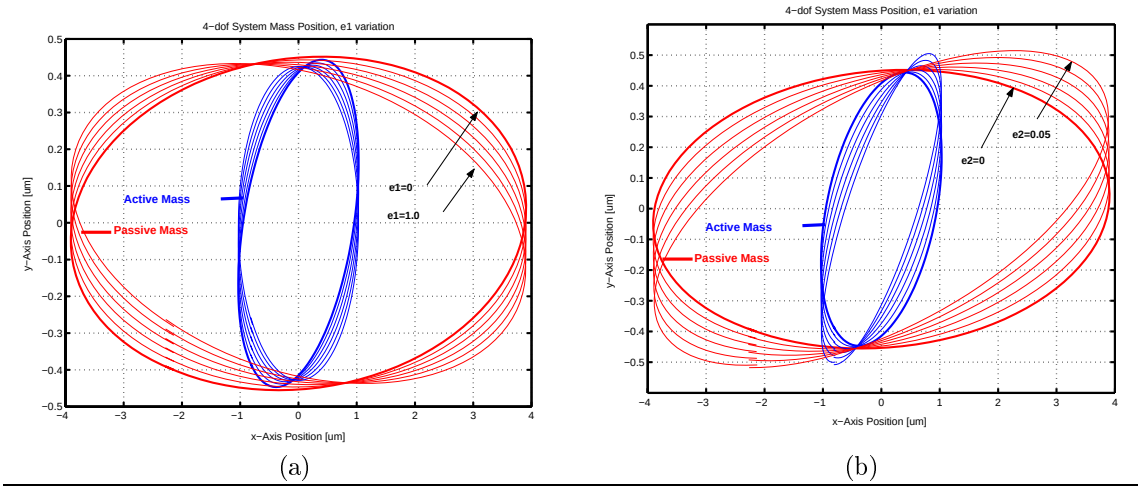

Figure 14. Oscillation patterns variation of the active and passive masses with (a) increasing ε_1 and (b) increasing ε_2.

Since the fabrication imperfection scatter is not symmetrical, the drive and sense axes in the gyroscope will not perfectly coincide with the principle axes of elasticity of the two suspension systems, which are the flexures between the active mass and the substrate, and flexures between the passive and active masses. The asymmetric imperfections can be modeled as an angle of elasticity ε_1 for substrate-active mass suspension, and ε_2 for active mass-passive mass suspension (Fig. 13). These angles will result in cross-coupling stiffness terms k_{1xy} and k_{2xy}, and the deviated stiffness terms $k_{1xx}, k_{2xx}, k_{1yy}$, and k_{2yy}.

$$
\begin{aligned}
k_{1xx} &= \frac{k_{1x}+k_{1y}}{2} + \frac{k_{1x}-k_{1y}}{2}cos(2\varepsilon_1) \qquad k_{1yy} = \frac{k_{1x}+k_{1y}}{2} - \frac{k_{1x}-k_{1y}}{2}cos(2\varepsilon_1) \qquad k_{1xy} = \frac{k_{1x}-k_{1y}}{2}sin(2\varepsilon_1) \\
k_{2xx} &= \frac{k_{2x}+k_{2y}}{2} + \frac{k_{2x}-k_{2y}}{2}cos(2\varepsilon_2) \qquad k_{2yy} = \frac{k_{2x}+k_{2y}}{2} - \frac{k_{2x}-k_{2y}}{2}cos(2\varepsilon_2) \qquad k_{2xy} = \frac{k_{2x}-k_{2y}}{2}sin(2\varepsilon_2)
\end{aligned} \tag{6}
$$

With the deviated stiffness values and the cross-coupling terms, the most general equation of motion for the non-ideal 4-DOF system can be expressed as:

$$
\begin{aligned}
m_1\ddot{x_1} + c_{1x}\dot{x_1} + c_{2x}(\dot{x_1}-\dot{x_2}) + k_{1xx}x_1 + k_{2xx}(x_1-x_2) &= k_{1xy}y_1 - 2m_1\Omega_z\dot{y_1} + F_d(t) \\
m_2\ddot{x_2} + c_{2x}(\dot{x_2}-\dot{x_1}) + k_{2xx}(x_2-x_1) &= k_{2xy}y_2 - 2m_2\Omega_z\dot{y_2} \\
m_1\ddot{y_1} + c_{1y}\dot{y_1} + c_{2y}(\dot{y_1}-\dot{y_2}) + k_{1yy}y_1 + k_{2yy}(y_1-y_2) &= k_{1xy}x_1 + 2m_1\Omega_z\dot{x_1} \\
m_2\ddot{y_2} + c_{2y}(\dot{y_2}-\dot{y_1}) + k_{2yy}(y_2-y_1) &= k_{2xy}y_1 + 2m_2\Omega_z\dot{x_2}
\end{aligned} \tag{7}
$$

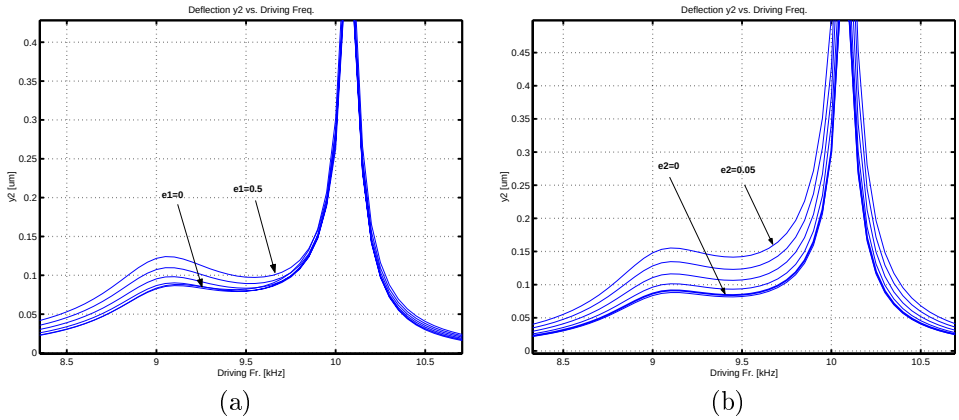

Figure 15: Effect of(a) ε_1 variation, and (b) ε_2 variation on 4-DOF system response.

When the anisoelasticity angles ε_1 and ε_2 are introduced to the system, phase changes are observed most significantly on x_1. Thus, anisoelasticity has the most effect on the trajectory of active mass, which is not the sensing element of the gyroscope. However, when critical values of the anisoelasticity angles ε_1 and ε_2 are exceeded, the passive mass sense amplitude increases, burying the contained Coriolis signal. It is also observed that the system is significantly immune to anisoelasticity in the active mass suspension, while the mass trajectories and gyroscope response is affected dramatically with anisoelasticity in the passive mass suspension (Fig. 15).

4. EXPERIMENTAL VERIFICATION OF THE DESIGN CONCEPT

To assure an accurate angular rate measurement, it is crucial that the sensing element of the gyroscope is sustained in a constant amplitude oscillation in the drive direction, since the Coriolis response is directly proportional to the drive direction oscillation amplitude. Preliminary experiments conducted on prototype dual-mass gyroscopes indicated a driving frequency range of over 2 kHz within where the drive direction oscillation amplitude varies by 10% (Fig. 17b). A conventional gyroscope design with similar geometry exhibited less than 200 Hz driving frequency range for 10% gain variation under same operating conditions, which is over 1.8 kHz less than dual-mass design operation range, verifying the drastically improved robustness of the dual-mass design.

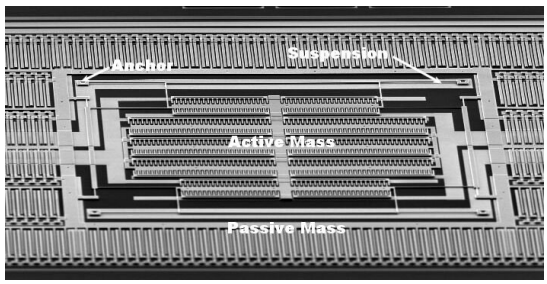

Figure 16: SEM photograph of the tested prototype gyroscope.

The prototype gyroscopes also successfully demonstrated the mechanical amplification of "master mass" oscillation by the "slave mass" , which is the sensing element of the gyroscope. The drive direction oscillation amplitude of the passive mass, which is one of the major parameters determining gyroscope performance, was demonstrated to be over 15 times larger than the active mass under atmospheric pressure (Fig. 17a). At the antiresonance frequency, the active mass drive amplitude (A_1 in Fig. 17a) was observed to be less than $0.1\mu m$, while the passive mass amplitude (A_2 in Fig. 17a) reached $1.4\mu m$.

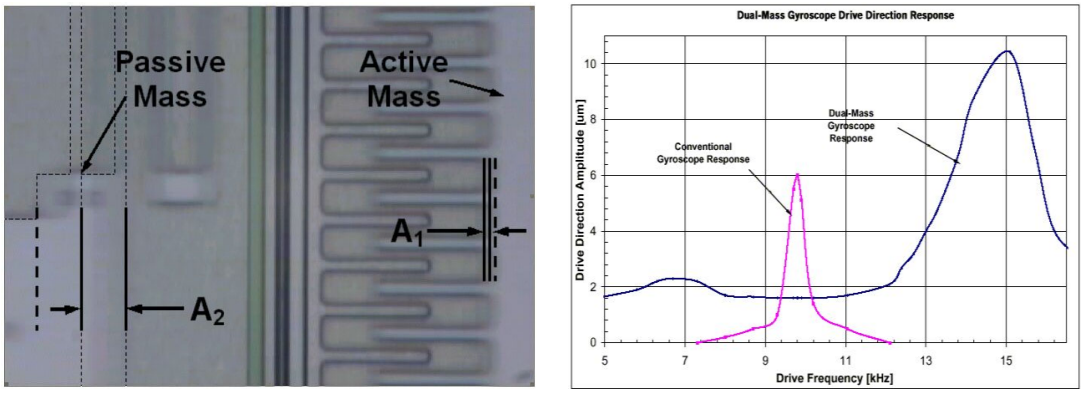

(a) (b)

Figure 17. (a) Demonstration of mechanical amplification in drive direction. The oscillation blur of the slave (passive) mass is highlighted. At the antiresonance frequency, the slave mass amplitude is over an order of magnitude larger than the master (active) mass amplitude. (b) Experimental verification of the wide constant-amplitude operation frequency band. 4-DOF system provides a constant-amplitude oscillation frequency band over 10 times larger than conventional gyroscopes under same operation conditions.

Moreover, the proposed system offers significant advantages in self-calibration schemes and control of the drive mode oscillations. Since the maximum mechanical amplification occurs at exactly the resonant frequency of the isolated second mass-spring system, the driving frequency was extracted from a reference resonator with the same geometry and parameters as the isolated second mass-spring system built in the vicinity of the dual-mass gyroscope. With a simple Phase-Locked Loop built around the resonator stabilizing the operation frequency to the resonant frequency, the driving signal of the gyroscope is obtained from the output of the voltage-controlled oscillator of the phase-locked loop. Since all parameter variations including residual stresses or fabrication imperfections will reflect on the reference oscillator in the exact same way, the driving frequency of the gyroscope will be locked in the nominal operation band automatically at all times, without the necessity of building feedback loop around the gyroscope itself, significantly simplifying control electronics compared to the conventional designs.

5. CONCLUSION

In this paper a novel concept for designing wide-bandwidth micromachined gyroscopes with improved robustness was reported, along with experimental demonstration of feasibility of implementation. Specifically, it was theoretically shown and experimentally demonstrated that, by utilizing the passive disturbance-rejection capability of the oscillatory system, improved robustness is achieved against parameter variations in gyroscope dynamics. The proposed design concept was verified to provide inherent insensitivity to fabrication variations, and fluctuations in the ambient temperature or pressure during the operation time of the device; requiring less demanding control strategies for operation under presence of perturbations. Thus, the new approach is projected to relax tight fabrication tolerances, and to result in reduced production cost of micromachined gyroscopes. These advantages will allow a wide range of low-cost inertial sensing applications, where the device will be subject to high fluctuations in operation conditions.

REFERENCES

1. N. Yazdi, F. Ayazi, and K. Najafi. Micromachined Inertial Sensors. *Proceedings of IEEE, Vol. 86, No. 8*, August 1998, pp. 1640-1658.
2. W.A. Clark, R.T. Howe, and R. Horowitz. Surface Micromachined Z-Axis Vibratory Rate Gyroscope. *Proceedings of Solid-State Sensor and Actuator Workshop*, June 1994, pp. 199-202.
3. E. Netzer, and I. Porat. A Novel Vibratory Device for Angular Rate Measurement. *Journal of Dynamic Systems, Measurement and Control, Vol. 117*, Dec. 1995, pp. 585-591.
4. A. Shkel, R.T. Howe, and R. Horowitz. Micromachined Gyroscopes: Challenges, Design Solutions, and Opportunities. *SPIE Conference on Smart Electronics and MEMS*, Newport Beach, 2001, pp. 74-85.
5. A. Shkel, R. Horowitz, A. Seshia, S. Park and R.T. Howe. Dynamics and Control of Micromachined Gyroscopes *American Control Conference, CA*, 1999, pp. 2119-2124.
6. C.W. Dyck, J. Allen, R. Hueber. Parallel Plate Electrostatic Dual Mass Oscillator. *Proceedings of SPIE Conference on Micromachining and Microfabrication, Vol. 3876, CA*, 1999, pp. 198-209.
7. C. Acar and A. Shkel. Micro-Gyroscopes with Dynamic Disturbance Rejection. *Proc. of SPIE Conference on Smart Electronics and MEMS*, Newport Beach, 2001, pp. 107-118.
8. C. Acar and A. Shkel. Wide Bandwidth Micromachined Gyroscope to Measure Rotation. *Patent pending, UCI Office of Technology Alliances*, Case No:2001-140-1.
9. A. Shkel, R.T. Howe, and R. Horowitz. Modeling and Simulation of Micromachined Gyroscopes in the Presence of Imperfections. *International Conference on Modeling and Simulation of Microsystems*, Puerto Rico, 1999, pp. 605-608.